Continuous wave protocol for simultaneous polarization and optical detection of P1-center electron spin resonance

E. J. Kamp, B. Carvajal, and N. Samarth

Phys. Rev. B **97**, 045204 — Published 10 January 2018

DOI: 10.1103/PhysRevB.97.045204

Continuous Wave Protocol for Simultaneous Polarization and Optical Detection of P1 Center Electron Spin Resonance

E.J. Kamp,[1,*] B. Carvajal,[1] and N. Samarth[1,†]

[1]*Department of Physics, 104 Davey Lab,*

The Pennsylvania State University, University Park PA 16802

(Dated: November 13, 2017)

Abstract

The ready optical detection and manipulation of bright nitrogen vacancy center spins in diamond plays a key role in contemporary quantum information science and quantum metrology. Other optically dark defects such as substitutional nitrogen atoms ('P1 centers') could also become potentially useful in this context if they could be as easily optically detected and manipulated. We develop a relatively straightforward continuous wave protocol that takes advantage of the dipolar coupling between nitrogen vacancy and P1 centers in type 1b diamond to detect and polarize the dark P1 spins. By combining mutual spin flip transitions with radio frequency driving, we demonstrate the simultaneous optical polarization and detection of the electron spin resonance of the P1 center. This technique should be applicable to detecting and manipulating a broad range of dark spin populations that couple to the nitrogen vacancy center via dipolar fields, allowing for quantum metrology using these spin populations.

Paramagnetic impurities in the solid state are a well-established platform for studies in quantum information and quantum metrology.[1] Nitrogen vacancy (NV) centers are particularly important in this context, with recent demonstrations of heralded entanglement, nanoscale nuclear magnetic resonance (NMR), and sub-picotesla magnetic field sensitivity.[2–5] These advances rely on the unique properties of the NV center that allow for optical spin initialization and readout via off-resonant continuous wave (CW) illumination.[6] Since NV centers have long spin coherence times at room temperature and can be manipulated in the few GHz frequency range, these defects lend themselves to a variety of measurement schemes.[7,8] However, these schemes rely on a unique set of transitions within the NV center that are shared only by a few other spin systems such as di-vacancies in silicon carbide.[9] Other defects present in diamond, such as substitutional nitrogen (P1 centers), also interact with the NV center population via the dipolar interaction, and are an important source of decoherence.[10–12] These spins are not necessarily harmful: they can also be a major resource for quantum information, serving as qubits, or they can be used to enhance the sensitivity of NV center based magnetometry.[13–15] Since P1 centers are optically 'dark,' they are not as readily accessed as NV centers. It is thus important to develop straightforward methods that allow for both polarization and detection of these dark spins for potential applications.

CW optically detected magnetic resonance (ODMR) has proven to be a powerful tool for the measurement of small magnetic fields using NV centers. Additionally, when CW ODMR is used with scanning probe NV center tools, it can provide a quick scheme for the measurement of magnetic properties.[16,17] In contrast, the methods for studying dark spins have primarily used pulsed electron spin resonance (ESR) protocols. For instance, double electron-electron resonance (DEER) has proven a versatile technique for detecting the resonance and coherence of dark spins.[13,15] Further, spin locking protocols have used the Hartman-Hahn condition to both polarize and detect dark spin populations.[15,18] The only demonstration thus far of CW detection of P1 centers uses cross-relaxation spectroscopy, but this approach is limited by the lack of polarization generated in the P1 centers, leading to a very small signal.[19,20]

In this article, we demonstrate a CW approach to polarizing the P1 center and we develop a means of detecting this polarization via the ensuing electron spin resonance (ESR) spectra. Recently, several features in the low field ODMR spectra of the NV center were studied and attributed to mutual spin flip transitions between the NV and the P1 center.[21] Here, we use

these transitions as well as optical pumping of the NV center to show that the polarization of the NV can be transferred to the P1 center. Our approach is distinct from previous ones that use mutual spin flip transitions to polarize nuclear spins due to the large difference in relaxation rates: our method exploits the tuneability of the NV center optical polarization rate to effectively increase the relaxation rate of the NV center. This allows us to move from a regime where the NV and P1 center relaxation rates are effectively the same to one where the NV center relaxes much more quickly, thus providing a means to generate polarization of the P1 center. Further, adding a driving field on the P1 center ESR transitions provides a way to translate the ESR into a detectable fluorescence change in the NV center.

The NV center is composed of a ground state and excited state triplet that are separated by 1.94 eV. Using off-resonant excitation (532 nm), we excite electrons from the ground state to the excited state through a phonon side band in a process that is mostly spin conserving. Electrons decay through one of two mechanisms, either spontaneous emission or non-radiative decay through an intersystem crossing composed of two singlet states. They then relax to the ground state with a slight preference into the $m_s = 0$ state. Because the coupling from the $m_s = \pm 1$ states to the intersystem crossing is slightly larger, this process leads to a buildup of polarization into the $m_s = 0$ state and additionally to a higher photoluminescence emission from the $m_s = 0$ state over the $m_s = \pm 1$ states, allowing for spin readout.

In these experiments, we focus on type Ib diamond which has N concentrations of between 100-200 ppm, leading to high density ensembles of both NV and P1 centers after electron irradiation. This high concentration leads to an average N-NV separation in the range of $3 - 5$ nm, leading to a large dipolar coupling between the two defect spins. The P1 center is composed of a spin 1/2 electron and a spin 1 nucleus. At zero field, these spins couple through the hyperfine interaction forming states of spin 1/2 and 3/2, where the spin 3/2 states split due to the lack of spherical symmetry in diamond.[22] These states couple to the triplet states of the NV center, leading to the energy spectrum shown in Fig. 1(a). Excitation with a weak microwave magnetic field only allows transitions where $\Delta(m_s) = \pm 1$ (shown in blue in Fig. 1 (a))). However, dipolar coupling introduces a small non-secular component to the system Hamiltonian, weakly allowing 'forbidden' transitions, where the total spin state of the system changes by $\Delta(m_s) = 0$ or $\Delta(m_s) = \pm 2$(transitions shown in red).[21]

Zero field ODMR measurements provide a means for detecting both the allowed and forbidden transitions in this system. In Fig. 1(b), we show the zero field ODMR spectrum for a sample with a high density of NV centers. At low microwave field amplitudes, only the transitions of the NV center are seen.[6] However, increasing the strength of the microwave field enhances the weaker forbidden transitions which manifest as two peaks equally spaced on either side of the central NV center resonance.[21]

Mutual spin flip transitions have been used in NMR to transfer thermal electron spin polarization to nuclear spins. This method is effective in the limit where the line width of the ESR transition is much smaller than the NMR frequency and when the electron spin lifetime is far smaller than the nuclear spin lifetime.[23] Here, we show that this technique can be used to transfer spin polarization between different electron spin populations. The first requirement is met here because the line width of the zero field ESR transition is on the order of tens of megahertz while the P1 center transitions are 131 MHz and 149 MHz, as can be seen in Fig. 1(b) where the sidebands are clearly resolved from the primary peak. (We ignore an additional resonance split by 36 MHz around the NV center zero field resonance and therefore not resolved.) The second requirement is less obvious because the spin lifetimes of both spin populations are of the same order of magnitude. We can, however, change the rate at which spins are pumped out of the ± 1 states by introducing optical pumping. This allows us to tune the effective rate at which spins are initialized by changing the laser power. As shown in Fig. 1(c), this allows us to tune the initialization rate from hundreds of microseconds down to the limit imposed by the intersystem crossing lifetime which is approximately 500 ns (see appendix A for details on the experimental procedure).

A toy model of the states relevant for this process allows us to gain an intuitive idea of the process that leads to spin polarization. If we focus on a single mutual spin flip transition, then the coupled NV-P1 system can be roughly approximated by two spin 1/2 electrons that are dipolar coupled. Figure 1(a) shows the relevant states for the process when driving on a zero quantum transition ($\Delta m = 0$) while optically pumping. The polarization of the P1 center is most easily understood in the limit where the optical pumping rate Γ_P is much larger than the spin relaxation rate of the P1 centers $\Gamma_{1,P1}$. In this limit, the combination of microwave driving and optical pumping will generate a large buildup of the spin population in the lowest energy state $|a\rangle$.

The simple picture that we use can be described by a two-spin Hamiltonian which includes

dipolar coupling and an AC magnetic field,

$$H = \omega_{0,NV} S_{z,NV} - \omega_{0,P1} S_{z,P1} + A S_{z,NV} S_{z,P1} + B S_{z,NV} S_{x,P1} + \omega_{1,NV} S_{x,NV}, \tag{1}$$

where $\omega_{0,NV}$ ($\omega_{0,P1}$) are the transition frequencies for the NV and P1 center spin populations, $S_{i,NV}$ ($S_{i,P1}$) are the spin operators in each basis and A and B are the secular and nonsecular components of the dipolar coupling and $\omega_{1,NV}$ is the Rabi frequency of the bare NV center transition proportional to the square of the microwave driving field. To obtain steady state spin populations for this system, we use Liouville's equation for the density operator $\hat{\rho}$:

$$\frac{d\hat{\rho}}{dt} = \frac{i}{\hbar}[H, \hat{\rho}] + \left\{ \frac{d\hat{\rho}}{dt} \right\}_{\text{relax}}. \tag{2}$$

We thus calculate the time evolution of the Hamiltonian phenomenologically, with the last term accounting for relaxation effects pertinent to the evolution of the system. It has previously been shown that this Hamiltonian can be reduced to one similar to that describing an AC field coupling a two level system.[24] For the zero quantum transition, the Hamiltonian,

$$H_{ZQ} = \frac{1}{2}\left\{ \Delta_{DNP}^{ZQ}(S_{NV,z} + S_{P1,z}) - \frac{\omega_{1,NV} B}{2\omega_{0,P1}}(S_{NV}^{+} S_{P1}^{-} + S_{NV}^{-} S_{P1}^{+}) \right\}, \tag{3}$$

resembles that for a two level system, but $\Delta_{DNP}^{ZQ} = \omega_m - (\omega_{0,NV} - \omega_{0,P1})$ is the detuning from the zero quantum resonance condition. The Rabi frequency, however, is modified to $\Omega_R = \frac{\omega_{1,NV} B}{2\omega_{0,P1}}$. Both spin relaxation and optical pumping are introduced as relaxation terms. Finally, we model the expected photoluminescence contrast using a formalism developed earlier.[25]

To test our model, we compare it with zero field ODMR measurements. Since optical pumping is the one of the primary generators of polarization, we compare the dependence of the sidebands on optical pumping with that of the central peak. In Fig. 2(a), we show zero field ODMR at three separate laser powers, revealing that the evolution of the sideband amplitude is different from that of the central peak. To generate a model to compare with our data, we used the procedures described in appendix A to measure the relevant parameters $T_1 = 51$ μs and $T_2 = 865$ ns of the NV center ensemble as well as the microwave driving field, $\omega_{1,NV} = 17$ MHz (using a magnetic field of 75 G to isolate a single orientation). We assume that T_1 for the P1 center is the same as that for the NV center ensemble.[10] Finally, we estimate the strength of the dipolar coupling to be about 2 MHz.[21] A comparison of the

resulting model with both the central peak and sideband peak amplitudes is seen in Fig. 2(b).

We first note that while the central peak contrast varies monotonically with initialization rate, with a strong decrease at low initialization rates, the sideband contrast shows non-monotonic behavior. It first increases as the initialization rate decreases before peaking and dropping off. This indicates that the sidebands have a lower Rabi frequency than the central peak, in agreement with the modified Rabi frequency proposed in our model.[26] A qualitative physical picture is obtained by considering the interaction between the optical pumping and Rabi flopping. In the limit where optical pumping is very slow compared with the Rabi frequency, the contrast is small due to the low polarization of the NV centers. As the optical pumping rate is increased, the contrast increases due to the increase in NV center polarization until the point where the optical pumping rate surpasses the Rabi frequency. In this limit, the contrast again decreases because spins are pumped into the excited state much faster than they are transferred into the $m_s = 1$ state. Comparison of the data (red points) to the model (black line) shows qualitatively reasonable agreement, though the model predicts a lower contrast. This shortcoming can be explained by considering that we only model two spins interacting via dipolar coupling; in reality, we are probing an ensemble of spins where both the NV center and the P1 center have four possible orientations each. Each orientation has a different Rabi frequency, as well as different PL emission (due to the axis between the dipole orientation and the laser polarization), and should therefore be described by distinct models. The overall signal would then be the sum of the four models, consistent with the lower signal expected from our model.

We estimate the polarization generated through the driving of mutual spin flip transition by comparing the spin populations predicted in our model with those expected from thermal polarization. Defining the polarization of our system as $P_{P1} = (\rho_a + \rho_c) - (\rho_b + \rho_d)$, we obtain a maximum possible polarization of 13% for our system parameters. Comparing this with the thermal polarization generated by a two state system with energy separation of 150 MHz, we find a predicted polarization enhancement of over 10^4 (Fig. 2(c)). Additionally, as expected, the polarization requires a strong optical pump to be effective. While the actual polarization achieved is likely lower due to charge state effects on NV center polarization, this represents a significant polarization enhancement.[27]

The transitions that generate P1 center polarization also provide an opportunity to op-

tically detect the ESR spectrum of the P1 center. Qualitatively, this can be seen in our toy model if we include a second RF microwave field. When this field is resonant with the P1 transition, the polarization no longer builds up in state $|a\rangle$, leading to a higher population in state $|c\rangle$ and thus a reduced fluorescence. This predicts an ODMR signal similar to that seen when driving a normal NV center transition. We can measure such an ODMR signal by detecting the fluorescence while simultaneously driving the mutual spin flip transition via a microwave field and the P1 center transition via an RF field (inset to Fig. 3(a)). We note that P1 center ESR has also been detected recently at low fields using cross relaxation spectroscopy where multiple quantum spin flip flop processes involving both the NV and P1 centers lead to a reduction in T_1 and thus a reduced PL emission from the NV center.[19] To distinguish the signal measured here from cross relaxation ODMR, we compare PL measured with the mutual spin flip driving both on and off: since cross relaxation only affects Rabi driving on the P1 transition, it will show up in both the signal and the reference, thus allowing us to subtract it out.

In Fig. 3(a), we demonstrate that simultaneous driving of the mutual spin flip transition and the P1 center transition gives an ODMR signal with three distinct peaks. For the data shown here, the microwave frequency was tuned to the zero quantum transition at 2.72 GHz. In order to confirm that the observed ODMR was the result of P1 center polarization generated via driving on the mutual spin flip transition, we repeated these measurements for decreasing microwave amplitudes. The decrease in the ODMR signal for lower microwave powers indicates the signal is a direct result of polarization of the P1 centers. From this observation we demonstrate that through driving of the mutual spin flip transition, we can simultaneously polarize and optically detect the P1 center electron spin resonance spectrum.

We fit the data using the sum of three Lorentzian peaks to determine the experimental values for the P1 center transition frequencies. To compare with the expected transition frequencies, we take the zero field Hamiltonian of the P1 center which only considers hyperfine coupling between the spin 1/2 electron and spin 1 nitrogen nucleus. This requires the parameters $A_{||}$ and $A_{\perp}$. For the measured resonances at 131 MHz and 149 MHz, the best values to use for those parameters are 114 MHz and 83 MHz, respectively, close to the values of 114 MHz and 82 MHz reported in the literature.[10,21,22] The third peak indicates coupling to an unknown spin population undergoing the same polarization and ODMR process as the P1 center.

In order to better understand the mechanism that generates an optical signature of the P1 center ESR spectrum, we also looked at the dependence of the optical contrast on the frequency used to generate polarization. To do this, we fixed the RF frequency to either 131 MHz (green data) or 149 MHz (blue data) and measured the peak amplitude while varying the frequency around the mutual spin flip transitions. Figure 3(b) shows that the amplitudes for the 131 MHz and 149 MHz transition are a maximum at separate mutual spin flip transitions. To understand this, we refer back to the diagram in Fig. 1(a) and consider a case with driving at two microwave frequencies f_1, tuned close to a mutual spin flip transition, and f_2, tuned near the P1 center ESR transition. When resonant with the P1 center ESR transition, the fluorescence is reduced because of a depletion in the population of state $|a\rangle$ and a redistribution of some of that population into state $|c\rangle$ which is the dimmer state of the NV center. This is most efficient when f_1 and f_2 are both coupled to the same state. This implies that the maximum contrast for the peak at 131 MHz and 149 MHz should occur at their respective mutual spin flip transitions as we see in Fig. 3(b). However, the inhomogeneous broadening is fairly large: this allows us to see both transitions as in Fig. 3(a). This frequency dependence further confirms our proposed mechanism for optical detection of the P1 center transitions and supports the predicted polarization generated through mutual spin flip transitions.

Finally, we investigate the properties of the polarization under a small magnetic field aligned to the (100) direction of the diamond sample. To calibrate the field magnitude and angle, we measured the ODMR spectra at low microwave powers. In this field configuration, we measured the high power ODMR spectra which shows the evolution of the sidebands. In order to determine the P1 center resonances, we fit both the high power spectra using a cubic polynomial background to account for the tails of the NV center resonance. The NV-ODMR spectra (red line) as well as the fit (black line) are shown in Fig. 4(a).

Using the NV-ODMR spectra, we measured the ESR spectra of P1 centers at low fields. In the NV-ODMR spectra, we see a mutual spin flip resonance at 2.72 GHz at 10 G and therefore use this driving frequency for our magnetic field measurements. With this driving frequency, we expect to simultaneously drive two transitions, one at a frequency of 146 MHz and one at 173 MHz, corresponding to sidebands of the $m_s = -1$ and $m_s = +1$ transitions, respectively. In Fig. 4(b), we do indeed see a transition near 173 MHz as well as a broader peak at a lower frequency. The lower frequency peak does not exactly correspond with the

146 MHz peak; however, there is an additional P1 transition at 134 MHz which, if weakly driven due to inhomogeneous broadening, could merge with the 146 MHz peak. This is possible given that inhomogeneous broadening at these microwave powers is much greater than 10 MHz and the peak width of the lower frequency resonance is much larger than that of the higher frequency resonance. Additionally, the peak at 155 MHz is still present, indicating that the unknown spin is only weakly Zeeman split, possibly indicating a nuclear spin system. In addition to a splitting of the peaks, we also see a decrease in the amplitude of the P1-ODMR peaks. The decrease in amplitude is expected from our model since the transition frequencies will decrease as the P1 transition frequencies increase, and agrees with the NV-ODMR measurements which show that the amplitude of the the sidebands has decreased significantly even by 10 G.

By fitting the spectra, we compare the measured resonances from the P1-ODMR, the high power NV-ODMR, and a model based on the P1 center Hamiltonian (Fig. 4(c)). We find reasonable agreement between the NV-ODMR measurements and the P1-ODMR measurements, but we also find some deviation from the model. We expect that the deviations of both our measurements from the model could be due to the uncertainty in both field and angle calculations based on the low power ODMR measurements of the NV center. Even with this deviation though, the agreement between the NV-ODMR and the P1-ODMR further shows that the sidebands allow us to polarize and measure ODMR spectra of the P1 center.

The polarization and contrast of our ESR signal are primarily limited by the strength of the microwave magnetic field on the mutual spin flip transition and the dipolar coupling strength. The first can be increased by building microwave devices directly on the sample and further optimizing the microwave system. In experiments that use on-chip microwave devices, driving frequencies of up to 440 MHz have been reported, an order of magnitude greater than our capabilities.[28] This would be particularly helpful when a magnetic field is introduced as the increased P1 center resonance frequency will reduce the Rabi frequency for the mutual spin flip transition. The second limitation, the dipolar coupling strength, is primarily limited by the separation between NV centers and P1 centers. By developing samples that start with higher nitrogen concentration, it should be possible to decrease the separation, although this will be accompanied by decreased T_1 and therefore require some optimization.

To summarize, we have demonstrated that using continuous wave microwave fields and optical pumping, we can generate efficient polarization of P1 centers in type Ib diamond. This polarization is mediated by mutual spin flip transitions that are allowed by weak dipolar coupling between the P1 and NV centers. Along with the polarization, we can optically measure the ESR transitions of the dark P1 centers, thus allowing for measurements of the properties of the P1 center spin bath. While this work focused on mutual spin flip driving on the P1 center, these techniques could be extended to any dark spin population which is strongly dipolar coupled to the NV center and could also be used in other systems such as defects in SiC.

We thank D. D. Awschalom for useful discussions. This work was supported by NSF DMR-1306510 (EK and NS) and by the NSF-REU program through DMR-1460920 (BC).

Appendix A: Experimental details

We carried out these measurements using a homebuilt microscope. We used a 532 nm laser with up to 200 mW of excitation power for initialization and readout of the NV center ensemble. For T_1 and T_2 spectroscopy, we used pulsed measurements wherein the laser was passed through an AOM in double pass configuration to generate short laser pulses, while also providing greater than 50 dBm of optical isolation for T_1 measurements. The laser was focused onto the sample using a Nikon 40×0.6NA objective lens that gave a spot size of $\sim 1\mu$m and an optical depth of $4 - 5\mu$m. The NV center photoluminescence (PL) was collected through the same objective and split off using a dichroic mirror with the $NV^{(-)}$ PL filtered using a 615 nm high pass filter. The PL was then collected using a avalanche photodiode (ID Quantique ID100) and the photons were gated using an SRS SR400 photon counter.

Microwaves were generated by one of two sources, either an SRS SG396 or an Agilent N9310A. For excitation of the NV centers, the microwaves were sent to a high speed switch (ZASWA-2-50r), amplified (Minicircuits ZHL-16W-43+), and delivered to a custom designed microwave stripline. In order to generate the large microwave fields necessary to resolve the mutual spin flip transitions, a 20μm gold wire was indium soldered to the sample. For low frequency excitation of the P1 centers, the microwaves were controlled through direct pulse modulation at the generator before being amplified (Minicircuits ZHL-20W-13SW+) and

delivered to the sample through a separate loop antenna placed under the sample. Control of all the pulse sequences was performed with a SRS SG645 pulse generator.

T_1 and T_2 measurements were performed using standard pulse sequences. For T_1 spectroscopy, the sequence began with a 100μs long optical pulse in order to initialize the NV centers into the $m_s = 0$ state. After a variable length wait time, the laser was turned back on and the PL was monitored during the first 1μs interval. In order to remove complications due to charge state fluctuations, a second sequence identical to the first but with a π pulse to transfer the spin state to the $m_s = -1$ state immediately after the optical initialization pulse. The data was then fit to a stretched exponential $C(t) = A * e^{(-(t/T_1)^{0.5})}$ due to the high concentration of nitrogen in the sample. T_2 measurements were performed using a standard spin echo sequence. Each of the measurements were repeated 10^6 times to accomulate the necessary statistics.

Measurement of the initialization rate was performed using a custom pulse sequence. In this sequence, an optical pulse was turned on and the PL was gated such that only photons from a short time period were collected. The optical pulse was followed by a wait period much longer than the measured T_1 time and with no laser excitation. By scanning the photon gate along the optical pulse, we were able to to follow the increase in photon emission associated with polarization into the $m_s = 0$ state. This sequence was then repeated 10,000 times in order to build up sufficient statistics for photon counting.

We used a two step lock-in measurement technique for the P1 center ODMR experiments. We define f_1 as the field tuned to the mutual spin flip transition and f_2 as the microwave field tuned near the P1 center transition. During the first measurement period, both the laser and the microwave at f_1 are supplied continuously while chopping f_2 and f_1. We keep track of two fluorescence signals, the signal S1, which is collected with f_2 on and the reference, R1, which is collected with f_2 off. The second measurement period is the same; however, we do not apply microwaves at f_1. We then define our final signal to be $\frac{S1}{R1} - \frac{S2}{R2}$. This subtraction allows us to eliminate any contribution to our signal that may arise due to cross relaxation.

Appendix B: Calculation of polarization enhancement and laser power dependence

Beginning with Eq. 1 introduced in the main text, we transform the Hamiltonian into one which resembles a two level Hamiltonian where the AC field is tuned to either the zero quantum or double quantum transition.[24] These calculations are valid under two limits, that $\omega_{0,P1} >> A/2$ and $B/2$, both of which apply in our case ($\omega_{0,P1} = 131$ and 149 MHz and A and B are of the order of MHz). For these calculations, we focus on the case of zero quantum driving as given by the Eq. 3. To incorporate optical pumping into our models, we define an optical pumping rate Γ_p which relaxes spins out of the $m_{s,NV} = \pm 1$ state. In order that our system is closed, we include all four states of the dipolar coupled NV-P1 center system. We can thus obtain equations which fully describe the spin state populations of our system. Here we show two examples,

$$\begin{aligned} \frac{d\hat{\rho_{bc}}}{dt} &= -i\Delta^{ZQ}_{DNP}\rho_{bc} - \frac{i\Omega_R}{2}(\rho_{cc} - \rho_{bb}) - \gamma_{NV}\rho_{bc}; \\ \frac{d\hat{\rho_{bb}}}{dt} &= -\frac{i\Omega_R}{2}(\rho_{cb} - \rho_{bc}) - \Gamma_{NV}(\rho_{bb} - \rho_{dd}) + \Gamma_p\rho_{dd} - \Gamma_{P1}(\rho_{bb} - \rho_{aa}), \end{aligned} \tag{B1}$$

where the state definitions are the same as defined in Fig. 1(a) of the text. Here, γ_{NV} describes the NV center transverse spin relaxation time, while Γ_i describes longitudinal spin relaxation of the corresponding spin population and Γ_p is the optical pumping rate. For the zero quantum case, only ρ_{bc} and ρ_{cb} are non zero (in the double quantum case ρ_{ad} and ρ_{da} are non zero). Finally, the steady state populations for each spin state are found by taking the time derivative to be zero and solving the resulting system of equations. The equations describing the population of states $|a\rangle$ and $|c\rangle$ are given by

$$\begin{aligned} \rho_{aa} &= \frac{2\Gamma_{P1}(\Gamma_{NV} + \Gamma_p)(2(\Gamma_{P1} + \Gamma_{NV}) + \Gamma_p)((\Delta^{ZQ}_{DNP})^2 + \gamma^2_{NV}) + \gamma_{NV}(\Gamma_{P1} + \Gamma_{NV} + \Gamma_p)^2\Omega^2_R}{(2(\Gamma_{P1} + \Gamma_{NV}) + \Gamma_p)[4\Gamma_{P1}(2\Gamma_{NV} + \Gamma_p)(\gamma^2_{NV} + (\Delta^{ZQ}_{DNP})^2) + \gamma_{NV}(2(\Gamma_{P1} + \Gamma_{NV}) + \Gamma_p)\Omega^2_R]} \\ \rho_{cc} &= \frac{2\Gamma_{P1}\Gamma_{NV}(2(\Gamma_{P1} + \Gamma_{NV}) + \Gamma_p)(\gamma^2_{NV} + (\Delta^{ZQ}_{DNP})^2) + \gamma(\Gamma_{P1} + \Gamma_{NV})(\Gamma_{P1} + \Gamma_{NV} + \Gamma_p)\Omega^2_R}{(2(\Gamma_{P1} + \Gamma_{NV}) + \Gamma_p)[4\Gamma_{P1}(2\Gamma_{NV} + \Gamma_P)(\gamma^2_{NV} + (\Delta^{ZQ}_{DNP})^2) + \gamma_{NV}(2(\Gamma_{P1} + \Gamma_{NV}) + \Gamma_p)\Omega^2_R]} \end{aligned} \tag{B2}$$

To check our that our steady state spin populations are consistent with the optical spin initialization properties of the NV center we look at the case of where $\Omega_R = 0$,

$$\rho_{aa} = \frac{\Gamma_{NV} + \Gamma_p}{2(2\Gamma_{NV} + \Gamma_p)}$$
$$\rho_{cc} = \frac{\Gamma_{NV}}{2(2\Gamma_{NV} + \Gamma_p)}. \tag{B3}$$

In the case of $\Gamma_p >> \Gamma_{NV}$ we get $\rho_{cc} = 0$ and $\rho_{aa} = 0.5$, consistent with full polarization due to optical pumping into the $m_{s,NV} = 0$ state. Additionally, in the case of $\Gamma_p = 0$ we obtain ρ_{aa} and $\rho_{cc} = 0.25$ consistent with equal population in each of our states.

We can find the polarization enhancement of the P1 center directly from the steady state spin populations. In our model, states $|a\rangle$ and $|c\rangle$ correspond to a single P1 center state and state $|b\rangle$ and $|d\rangle$ to the other. We therefore calculate the P1 center polarization as described in the main text and obtain,

$$P_{P1} = \frac{\gamma\Gamma_p\Omega_R^2}{4\gamma_{P1}(2\Gamma_{NV} + \Gamma_p)(\gamma_{NV}^2 + (\Delta_{DNP}^{ZQ})^2) + \gamma_{NV}(2(\Gamma_{P1} + \Gamma_{NV}) + \Gamma_p)\Omega_R^2]}, \tag{B4}$$

where the polarization can be seen to go to zero for both $\Omega_R = 0$ and $\Gamma_p = 0$ as we would expect.

In order to create a model of the laser power dependence, we utilize the formalism developed by Dreau *et. al.*.[25] To do this we phenomenologically account for spin state dependent PL emission by defining the overall photon emission rate to be,

$$R(\Omega_R, \omega_m, \Gamma_p) = \alpha(\rho_{aa}^{st} + \rho_{bb}^{st}) + \beta(\rho_{cc}^{st} + \rho_{dd}^{st}), \tag{B5}$$

where α and β are the photon emission rates from the $m_{s,NV} = 0$ state and $m_{s,NV} = \pm 1$ states respectively. Given that the $m_{s,NV} = 0$ emits at a higher rate, we restrict ourselves to the case where $\alpha > \beta$. In our experiments, ODMR is measured by normalizing the PL measured with the microwave on by the PL measured with the microwave are off. The contrast is therefore,

$$\begin{aligned} Contrast &= \frac{R(0,0,\Gamma_p) - R(\Omega_R, \omega_m, \Gamma_p)}{R(0,0,\Gamma_p)} \\ &= \frac{(\alpha - \beta)\Gamma_{P1}\Gamma_p\Omega_R^2}{(\beta\Gamma_{NV} + \alpha(\Gamma_{NV} + \Gamma_p))[4\gamma_{NV}\Gamma_{P1}(2\Gamma_{NV} + \Gamma_p) + (2(\Gamma_{P1} + \Gamma_{NV}) + \Gamma_p)\Omega_R^2]} \end{aligned} \tag{B6}$$

We can thus use the steady state populations to obtain the contrast. For Fig.2(b), we have set $\frac{\beta}{\alpha} = 0.7$ based on fits of the central peak data using the model developed by Dreau *et. al.* for ODMR contrast of allowed transitions.

---

* ejk216@psu.edu

† nsamarth@psu.edu

[1] D. D. Awschalom, L. C. Bassett, A. S. Dzurak, E. L. Hu, and J. R. Petta, Science **339**, 1174 (2013).

[2] G. Balasubramanian, I. Y. Chan, R. Kolesov, M. Al-Hmoud, J. Tisler, C. Shin, C. Kim, A. Wojcik, P. R. Hemmer, A. Krueger, T. Hanke, A. Leitenstorfer, R. Bratschitsch, F. Jelezko, and J. Wrachtrup, Nature **455**, 648 (2008).

[3] J. R. Maze, P. L. Stanwix, J. S. Hodges, S. Hong, J. M. Taylor, P. Cappellaro, L. Jiang, M. V. G. Dutt, E. Togan, A. S. Zibrov, A. Yacoby, R. L. Walsworth, and M. D. Lukin, Nature **455**, 644 (2008).

[4] T. Wolf, P. Neumann, K. Nakamura, H. Sumiya, T. Ohshima, J. Isoya, and J. Wrachtrup, Phys. Rev. X **5**, 041001 (2015).

[5] H. J. Mamin, M. Kim, M. H. Sherwood, C. T. Rettner, K. Ohno, D. D. Awschalom, and D. Rugar, Science **339**, 557 (2013).

[6] A. Gruber, A. Dräbenstedt, C. Tietz, L. Fleury, J. Wrachtrup, and C. v. Borczyskowski, Science **276**, 2012 (1997).

[7] G. Balasubramanian, P. Neumann, D. Twitchen, M. Markham, R. Kolesov, N. Mizuochi, J. Isoya, J. Achard, J. Beck, J. Tissler, V. Jacques, P. R. Hemmer, F. Jelezko, and J. Wrachtrup, Nat. Mater. **8**, 383 (2009).

[8] F. Jelezko, T. Gaebel, I. Popa, A. Gruber, and J. Wrachtrup, Phys. Rev. Lett. **92**, 076401 (2004).

[9] A. L. Falk, B. B. Buckley, G. Calusine, W. F. Koehl, V. V. Dobrovitski, A. Politi, C. A. Zorman, P. X. L. Feng, and D. D. Awschalom, Nat. Commun. **4**, 1819 (2013).

[10] S. Takahashi, R. Hanson, J. van Tol, M. S. Sherwin, and D. D. Awschalom, Phys. Rev. Lett. **101**, 047601 (2008).

[11] V. M. Acosta, E. Bauch, M. P. Ledbetter, C. Santori, K.-M. C. Fu, P. E. Barclay, R. G.

Beausoleil, H. Linget, J. F. Roch, F. Treussart, S. Chemerisov, W. Gawlik, and D. Budker, Phys. Rev. B **80**, 115202 (2009).

[12] E. E. Kleinsasser, M. M. Stanfield, J. K. Q. Banks, Z. Zhu, W.-D. Li, V. M. Acosta, H. Watanabe, K. M. Itoh, and K.-M. C. Fu, Appl. Phys. Lett. **108**, 202401 (2016).

[13] A. O. Sushkov, I. Lovchinsky, N. Chisholm, R. L. Walsworth, H. Park, and M. D. Lukin, Phys. Rev. Lett. **113**, 197601 (2014).

[14] H. S. Knowles, D. M. Kara, and M. Atatüre, Phys. Rev. Lett. **117**, 100802 (2016).

[15] C. Belthangady, N. Bar-Gill, L. M. Pham, K. Arai, D. Le Sage, P. Cappellaro, and R. L. Walsworth, Phys. Rev. Lett. **110**, 157601 (2013).

[16] M. Pelliccione, A. Jenkins, P. Ovartchaiyapong, C. Reetz, E. Emmanouilidou, N. Ni, and A. C. Bleszynski Jayich, Nat. Nanotechnol. **11**, 700 (2016).

[17] L. Rondin, J. P. Tetienne, S. Rohart, A. Thiaville, T. Hingant, P. Spinicelli, J. F. Roch, and V. Jacques, Nat. Commun. **4**, 2279 (2013).

[18] A. Laraoui and C. A. Meriles, Nano. Lett. **7**, 3403 (2013).

[19] H.-J. Wang, C. S. Shin, S. J. Seltzer, C. E. Avalos, A. Pines, and V. S. Bajaj, Nat. Commun. **5**, 4135 (2014).

[20] L. T. Hall, P. Kehayias, D. A. Simpson, A. Jarmola, A. Stacey, D. Budker, and L. C. L. Hollenberg, Nat. Commun. **7**, 10211 (2016).

[21] M. Simanovskaia, K. Jensen, A. Jarmola, K. Aulenbacher, N. Manson, and D. Budker, Phys. Rev. B **87**, 224106 (2013).

[22] W. V. Smith, P. P. Sorokin, I. L. Gelles, and G. J. Lasher, Phys. Rev. **115**, 1546 (1959).

[23] C. D. Jeffries, Phys. Rev. **117** 1056 (1960).

[24] B. Corzilius, A. A. Smith, and R. G. Griffin, J. Chem. Phys. **137**, 054201 (2012).

[25] A. Dréau, M. Lesik, L. Rondin, P. Spinicelli, O. Arcizet, J.-F. Roch, and V. Jacques, Phys. Rev. B **84**, 195204 (2011).

[26] E. Bourgeois, A. Jarmola, P. Siyushev, M. Gulka, J. Hruby, F. Jelezko, D. Budker, and M. Nesladek, Nat.Commun. **6**, 8577 (2015).

[27] M. Loretz, H. Takahashi, T. F. Segawa, J. M. Boss, and C. L. Degen, Phys. Rev. B **95**, 064413 (2017).

[28] G. D. Fuchs, V. V. Dobrovitski, D. M. Toyli, F. J. Heremans, and D. D. Awschalom, Science **326**, 1520 (2009).

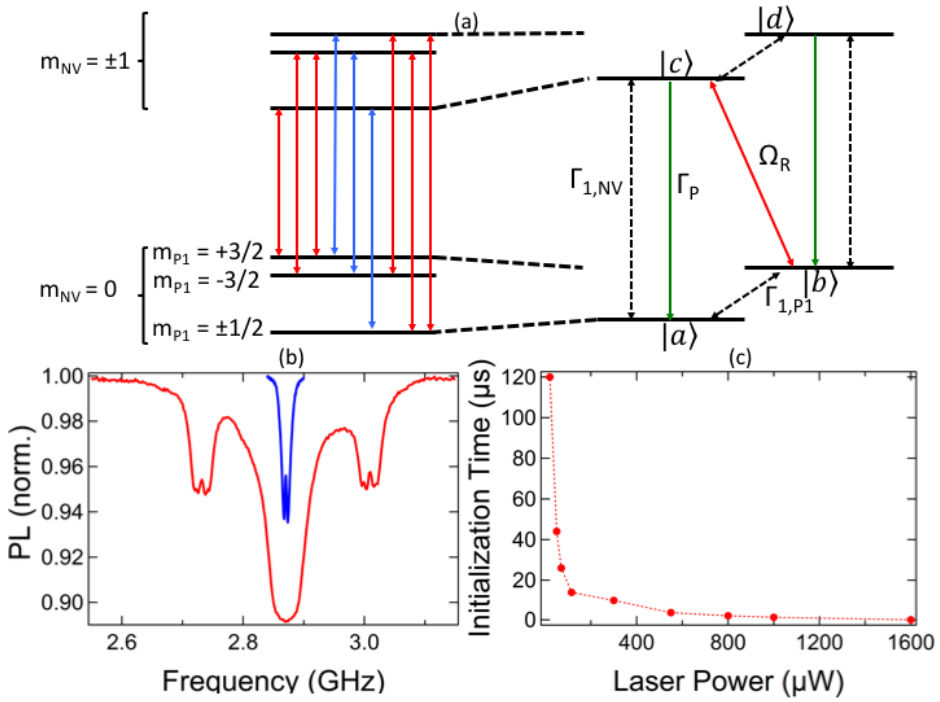

FIG. 1. Relevant energy levels and ODMR spectra at zero field. (a) At zero field, the energy levels of the coupled NV-P1 center system are composed of a spin 1 NV center and a spin 3/2 P1 center. Blue transitions are the normally allowed transitions, while the red transitions are forbidden transitions allowed by the dipolar coupling. In our model, we consider four of the six states. Here, we show one example, where we are driving a zero quantum transition between states $|b\rangle$ ($|m_{NV} = 0, m_{P1} = 3/2\rangle$) and $|c\rangle$ ($|\pm 1, \pm 1/2\rangle$). By including states $|a\rangle$ ($|0, \pm 1/2\rangle$) and state $|d\rangle$ ($|\pm 1, 3/2\rangle$) we are able to account for optical pumping and spin relaxation. (b) Zero field ODMR spectra of the NV center. Blue lines are at low microwave field amplitude, while red lines are at high microwave field amplitude. The forbidden transitions appear in the high field data as sidebands. (c) Dependence of the NV center spin initialization rate on laser power, showing large tuneability as well as a saturation at the intersystem crossing lifetime of 500ns.

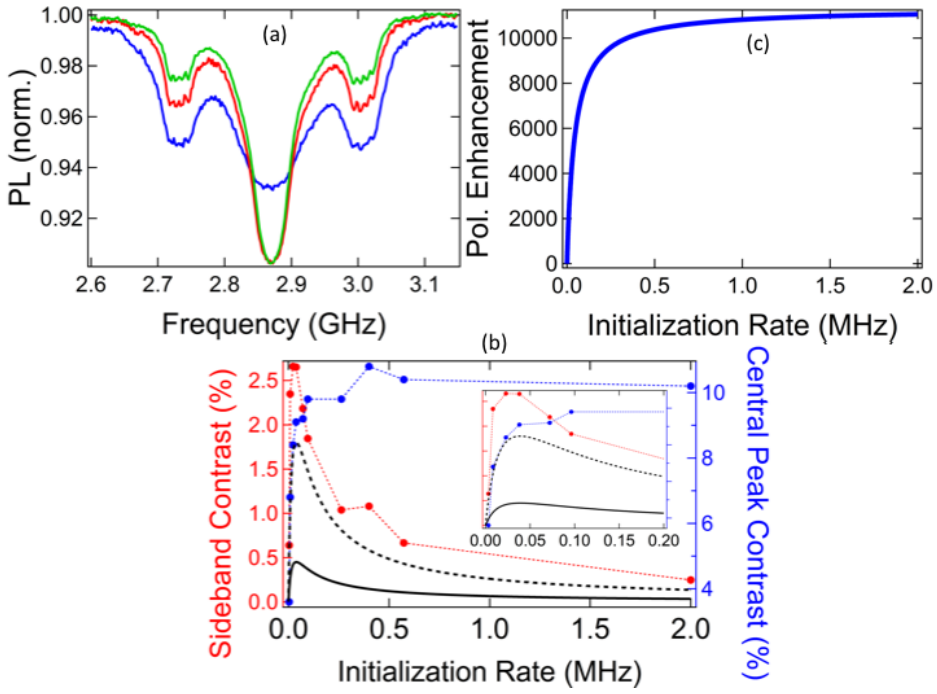

FIG. 2. Comparison of models with zero field optically detected magnetic resonance. (a) Zero field ODMR data at three different laser powers, 20 μW (blue), 300 μW (red), and 550 μW (green).(b) Dependence of the both the sideband (red) and central peak (blue) contrast on the initialization rate of the NV center. Black line shows a model using measured parameters for the NV center ensemble. Dashed black is the sum of four of the same model demonstrating what our model would look line for an ensemble. Inset: A closer look at the behaviour at low initialization rates where the vertical axes are the same as in the primary figure. (c) Polarization enhancement of the P1 center calculated from our models with the same parameters used to model the initialization rate dependence.

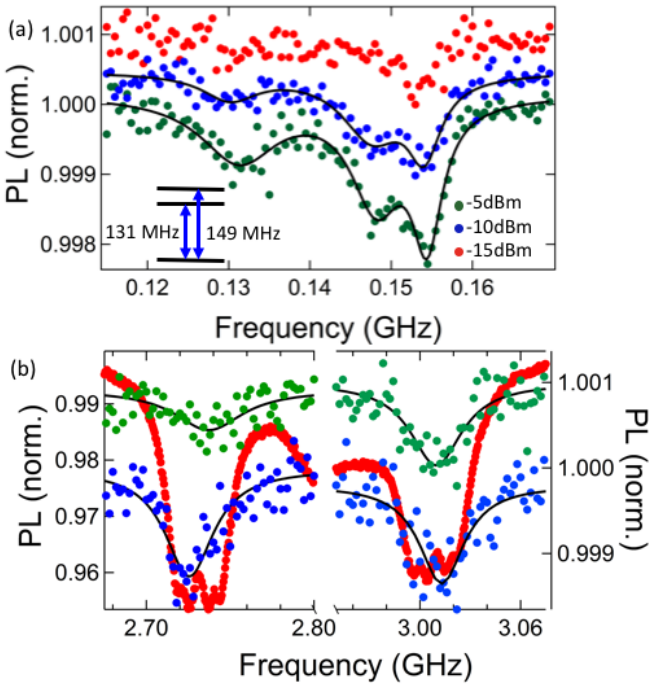

FIG. 3. Optically detected ESR spectra of the P1 center. (a) Optically detected ESR spectra of the P1 centers with driving on the zero quantum transition at 2.72Ghz. The dependence of the signal amplitude on the microwave field driving the mutual spin flip transition demontrates that the signal is a result of electron spin resonance of polarized P1 centers. Inset: zero field energy level of the P1 center assuming hyperfine coupling parameters of $A_{\|} = 114$ MHz and $A_{\perp} = 82$ MHz. (c) Driving field dependence of the optically detected P1 ESR spectra showing that the signal is maximum when the driving frequency is resonant with the corresponding mutual spin flip transition. Green data is taken centered on the P1 ESR peak at 131 MHz and the blue data is taken centered on the 149 MHz peak. Red data is the NV center ODMR data taken near the zero quantum resonance condition

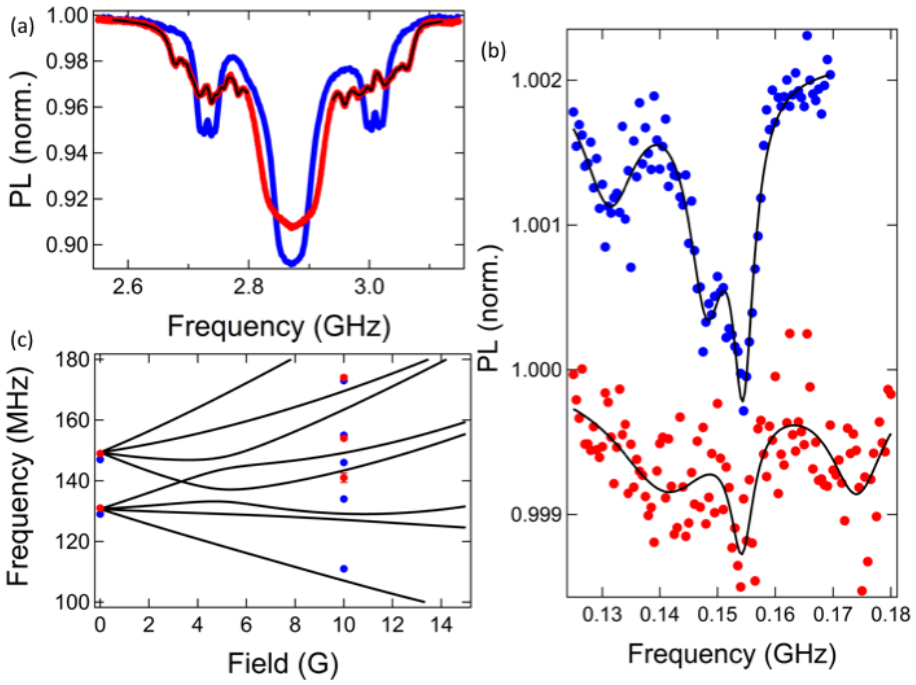

FIG. 4. Magnetic field dependence of the P1 center ESR spectra. (a) NV center ODMR spectra measured using a microwave Rabi frequency of 20 MHz. Here we show a comparison of the zero field data (blue) and data at 10 G (red) as well as the fit used to calculate the P1 center resonance frequencies (black line). (b) P1-ODMR comparison at 0 and 10 G. This data shows that with an applied field, the resonance splits and the amplitude decreases in agreement with our models. (c) Comparison of the NV-ODMR (blue dots), P1 ODMR (red dots) and a model of the P1 center (black lines). The measured peaks show good agreement but some deviation from the model.